ISSN (Print) 1226-1750
ISSN (Online) 2233-6656
Journal of Magnetics 23(1), 79-85 (2018) https://doi.org/10.4283/JMAG.2018.23.1.079

Tailoring the Impact Toughness of Sintered NdFeB Magnets via Surface Coating

X. G. Cui[1], J. X. Pan[1], C. Y. Cui[1]*, P. Mei[1], X. H. Wang[1], C. Fang[1], T. Y. Ma[2], C. Wang[3], and X. C. Peng[1]

[1]School of Mechanical Engineering, Jiangsu University, Zhenjiang 212013, PR China
[2]Department of Materials Science and Engineering, State Key Laboratory of Silicon Materials, Zhejiang University, Hangzhou 310027, PR China
[3]College of Materials Science and Engineering, Fuzhou University, Fuzhou 350108, PR China

(Received 22 November 2017, Received in final form 6 February 2018, Accepted 7 March 2018)

Metallic coating by electroplating is commonly attractive for improving the corrosion resistance of sintered NdFeB magnets. However, its tailoring of mechanical characteristics for sintered NdFeB magnets has been seldom concerned. Herein, the impact toughnesses of sintered NdFeB magnets with various metallic coatings (Ni or Ni/Sn) were comparatively investigated. The results indicate that the impact toughnesses of sintered NdFeB magnets are both improved by Ni coating and Ni/Sn bilayer coating. And Ni/Sn bilayer coating exhibits more enhancement of the impact toughness, increased by 41.6 % compared with the original magnet. Moreover, the microstructural observations of the metallic coatings and the fracture were conducted, and the enhanced mechanism of impact toughness for the magnet is analyzed. These findings may provide a reference for toughening the brittle materials.

Keywords : sintered NdFeB magnets, metallic coating, impact toughness, microstructure, fractography

1. Introduction

Sintered NdFeB magnet possesses superior magnetic properties and has attracted significant attention in recent years [1-3]. However, it tends to undergo the intergranular brittle fracture under the load due to the strong uniaxial magnetocrystalline anisotropy, few slip system and weak Nd-rich grain boundary phase [4]. Therefore, its toughness is very poor, seriously limiting its further application in the numerous load-bearing fields.

Many studies have conducted for exploring the effective methods to enhance the mechanical properties of sintered NdFeB magnets, especially the impact toughness [5-7]. It has been reported that the impact toughness of sintered NdFeB magnets can be rapidly improved by increasing Nd content ranging from 14.6 at.% to 22 at.%, but the magnetic properties are significantly decreased due to the more nonmagnetic phase [8-10]. Moreover, the addition of other metallic elements has also adopted for trying to improve the impact toughness of sintered NdFeB magnets. Previous reports indicate that the impact toughness can be effectively improved by properly adding the refractory metallic elements (Nb, Ti, Mo or W) [8, 11]. This may be attributed to the refined grains and the formed grain boundary phase. Furthermore, the co-additions of high- and low-melting metallic elements can simultaneously modify the matrix and Nd-rich phases, thereby leading to the improved impact toughness [12]. Besides aforementioned alloying method, the optimized fabrication process of sintered NdFeB magnets can contribute to the improvement of impact toughness as well. Our studies prove that dehydrogenation during powdering process can obviously increase the impact toughness of sintered NdFeB magnet [7]. In addition, the magnet prepared by spark plasma sintering (SPS) presents higher impact toughness than the conventional sintered magnet [13].

Coating is a common and effective method to protect sintered NdFeB magnets from corrosion. Up to now, most researchers have paid their attention to the effect of coating on the magnetic properties and corrosion resistance of NdFeB magnets [14, 15]. Nevertheless, the tailoring role of the coating, especially metallic coating, on the mechanical characteristics of sintered NdFeB magnets has been seldom concerned. And the related mechanism has been still unclear. Therefore, in this work, the effects of metallic coatings by electroplating on the impact toughness

*Corresponding author: Tel: +86-511-88797898
Fax: +86-511-88780241, e-mail: ccyyy981206@163.com

of sintered NdFeB magnets were investigated, and the relevant mechanism was analyzed on the basis of microstructural observation. This work may experimentally guide the improvement of the toughness of the brittle materials.

2. Experimental Procedures

A commercial NdFeB sintered magnet was used as the original magnet. The bulk magnet was cut into the impact samples with dimensions of 55 mm × 10 mm × 10 mm (l × w × h) by spark machining, l of which is along the aligned direction of magnet (Fig. 1). Prior to electroplating, the sample surfaces were pretreated through grinding, polishing, degreasing, pickling, cleaning, etc. Then, the Ni coating and Ni/Sn bilayer coating were electroplated on the pretreated samples, and their thicknesses were controlled by the electroplating time. The Ni coating was obtained from a bright acidic nickel bath basically comprising 300 g/L nickel sulfate hexahydrate, 40 g/L nickel chloride hexahydrate and 40 g/L boric acid at a temperature of 50 ℃. The Ni/Sn bilayer coating was obtained through further electroplating Sn from a sulfate bath with the basic constituents of 30 g/L stannous sulfate and 120 g/L sulfuric acid at a temperature of 20 ℃ on the aforementioned Ni coating. Finally, the coatings were washed and dried for further characterization.

The impact toughnesses of the samples without and with metallic coatings were measured using a Charpy impact method. The crystal structures of both coatings were identified by a Rigaku D/Max-2550pc diffractometer (Cu Kα, radiation). The surface morphologies of the coatings and the fracture morphologies of the samples were observed under a HITACH S-4800 scanning electron microscope (SEM) equipped with an energy dispersive X-ray spectrometer (EDS). The elemental analysis of the sample was performed using EDS spot scan mode.

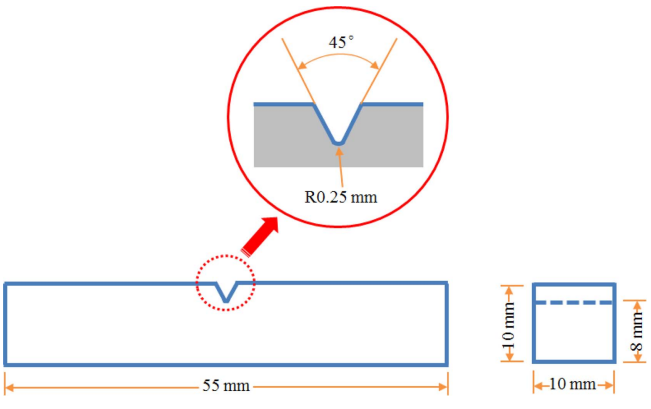

Fig. 1. (Color online) Schematic diagram of the impact specimen.

3. Results and Discussion

3.1. Surface morphology and structure analysis

Figure 2 shows the surface morphologies of Ni and Ni/Sn coatings. The Ni coating is compact and smooth, exhibiting the cellular structure (Fig. 2(a)). However, the top Sn coating in Ni/Sn bilayer coating presents a different surface morphology. It appears relatively flat and mirror-like, and no grain structure can be observed, as shown in Fig. 2(b). This is consistent well with the reported surface morphology of Sn coating in the literature [16]. The different morphologies between Ni and Sn coatings may suggest their different microstructures, thereby displaying the different mechanical behavior during the impact test.

The crystal structure and microstructure of Ni and Ni/Sn coatings are further characterized by the XRD measurements. Figure 3 depicts the XRD patterns of the Ni coating and the top Sn coating in Ni/Sn bilayer coating in Fig. 2. The diffraction peaks of both coatings are clearly distinguishable. The main diffraction peaks of Ni coating are (111), (200) and (311) etc., and those of top Sn coating are (112), (101) and (211) etc., demonstrating the characteristic reflections of Ni and Sn crystal lattices. According to the standard PDF cards, the crystal structures of Ni and top Sn coatings can be indexed to the face-

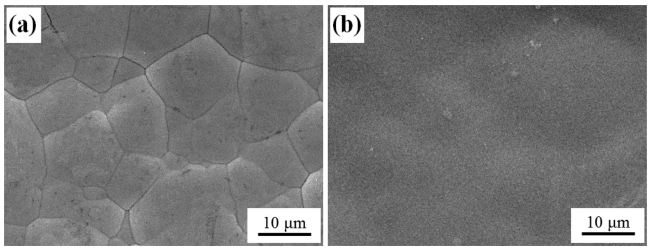

Fig. 2. SEM images of the coatings: (a) Ni coating; (b) Sn coating in Ni/Sn bilayer coating.

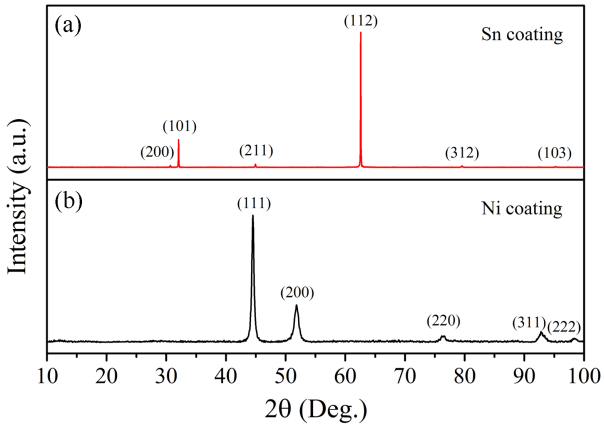

Fig. 3. (Color online) XRD patterns of the coatings: (a) Ni coating; (b) Sn coating in Ni/Sn bilayer coating.

centered cubic (FCC) Ni (JCPDS No. 04-0850) and body-centered tetragonal (BCT) Sn (JCPDS No. 04-0673). However, the intensities of the main peaks for Ni and Sn coatings change more or less, indicating the variation of the crystal orientation. This has been proved to be an important factor affecting the mechanical characteristics of the coating [17].

The preferred orientation of both coatings can be evaluated by the texture coefficient (*TC*), which is estimated from the XRD data according to the following equation [18]:

$$TC(\mathrm{hkl}) = \frac{I(\mathrm{hkl})/I_0(\mathrm{hkl})}{\frac{1}{n}\Sigma I(\mathrm{hkl})/I_0(\mathrm{hkl})} \quad (1)$$

where *TC*(hkl) is the texture coefficient of the (hkl) plane, *I*(hkl) and I_0(hkl) are the measured peak intensity and the relative peak intensity of the (hkl) plane taken from the standard PDF cards, and n is the total number of the peaks considered. *TC*(hkl) greater than one implies the preferred orientation of the (hkl) plane. On the basis of Eq. (1), *TC* of the crystal planes in above diffraction patterns for Ni and Sn coatings are calculated and displayed in Fig. 4. As can be seen, the largest *TC*(hkl) of Ni coating is *TC*(111), suggesting the preferred crystal orientation along [111] direction. In addition, the ratio of the relative intensities for (111) and (200) peaks is 3.40, much larger than the theoretical ratio (2.38) of the corresponding peak intensities obtained from the standard PDF cards. This also confirms the preferred crystal orientation of (111) plane. The formation of (111) texture for Ni coating accords with the crystallization principle of the surface energy minimization. In FCC structure of Ni, the atomic density of (111) plane is higher than that of (200) plane, consequently the surface energy of (111) plane is lower than that of (200) plane. Ni atoms incline to crystallization in the (111) plane for minimizing the surface energy, thereby forming the (111) texture. This texture may result in the lower ductility and the higher hardness of Ni coating [19]. Likewise, the largest *TC*(112) of Sn coating indicates its (112) preferred crystal orientation. Moreover, compared with *TC*(112), *TC*s of other planes of Sn coating are very small and can be almost negligible, demonstrating that (112) preferred orientation is prominent. Besides, the broader diffraction peaks of Ni coating suggest the smaller grain size than that of the Sn coating. According to the Debye-Scherrer equation [20], the grain sizes are calculated through (111) and (200) diffraction peaks for Ni coating and (112) and (101) diffraction peaks for Sn coating, respectively. The average grain size of Ni coating is 13.8 nm, and that of Sn coating is 115.9 nm. Although the average grain size of Sn coating exceeds the calculable upper limit of the Debye-Scherrer equation, it still can illustrate that the Sn coating is composed of the coarser grains. Overall, Ni and Sn coatings have different crystal structures, textures and microstructures. This may result in different effects on the mechanical property of sintered NdFeB magnets.

3.2. Impact toughness and fractography analysis

In order to evaluate the effects of various coatings on the mechanical property of sintered NdFeB magnets, the analyses of impact toughness have been performed for the original and coated magnets. Figure 5 illustrates the impact toughness of the original magnet and the coated magnets with the Ni and Ni/Sn bilayer coatings. The impact toughness (α_k) is deduced through dividing the impact energy (A_k) by the minimum cross-sectional area of the sample [11]. It can be found that the metallic coating significantly increases the impact toughness of NdFeB magnet, especially

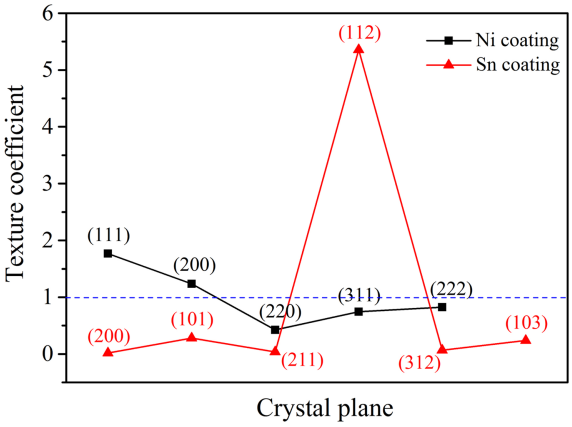

Fig. 4. (Color online) Texture coefficients of different crystal planes for Ni and Sn coatings.

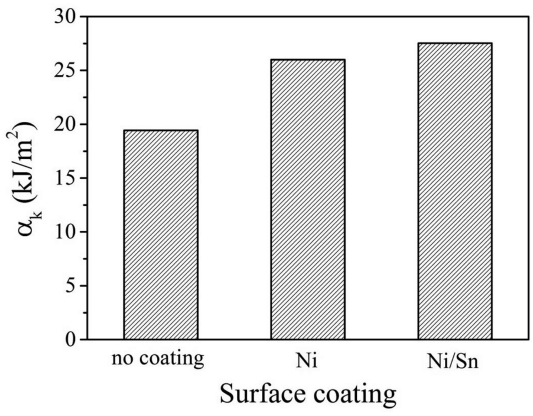

Fig. 5. Impact toughness of the original magnet and the coated magnets with the Ni coating and Ni/Sn bilayer coating.

the bilayer metallic coating. As for the Ni coating, the impact toughness of magnet is increased by 33.8 %. In contrast, the Ni/Sn bilayer coating is more effective to improve the impact toughness of magnet, the improvement of which attains 41.6 %. This exhibits an increasing trend in the impact toughness with increasing the coating layer number. But the improved effect is not as large as the expectation resulting from the multilayer coating, which may be correlated with the different effects of each coating with different crystal structures and microstructures. By comparison, the contributions of underlying Ni coating and top Sn coating in Ni/Sn bilayer coating to the impact toughness are actually different. It can be deduced through eliminating the role of underlying Ni coating that the increment of impact toughness induced by top Sn coating is much lower than that of underlying Ni coating. One of important reasons for the better toughening of Ni coating is that Ni with FCC structure possesses the superior intrinsic mechanical properties (strength and toughness) over Sn with BCT structure [21]. On the other hand, the grain size and texture also play important role [22]. Therefore, the impact toughness of NdFeB magnet can be more effectively enhanced through depositing the optimized metallic coating.

To find out the influence mechanisms of the various coatings on the impact toughness of sintered NdFeB magnet, the fracture surfaces of the coated NdFeB magnets with Ni and Ni/Sn bilayer coatings are analyzed. Figure 6 shows the fractography of Ni and Ni/Sn coated NdFeB magnets and EDS analyses of NdFeB substrate and Ni layer in Ni/Sn coating. It can be observed from Figs. 6(a) and (b) that the fracture behaviors of the metallic coatings and NdFeB substrate are significantly different. The fracture surface of NdFeB substrate is composed of polygonal $Nd_2Fe_{14}B$ grains characterized by EDS spectrum (Fig. 6(c)), exhibiting the rock sugar-like fracture morphology. Therefore, NdFeB substrate still appears typical intergranular fracture, which is the same as the fracture mode of the original NdFeB magnet (Fig. 7). The weak Nd-rich phase distributed along the grain boundaries is the main reason for the intergranular fracture of the magnet [4]. This indicates that although the metallic coating greatly improves the impact toughness, it cannot change the intrinsic fracture mechanism of sintered NdFeB magnet. Therefore, the improvements of impact toughnesses of the coated NdFeB magnets are mainly derived from the contributions of the metallic coatings. Figure 6(a) illustrates that the fracture surface of Ni coating is smooth and no noticeable area reduction can be observed, indicating that the fracture mode of nanocrystalline Ni (13.8 nm) coating may be predominantly intergranular fracture. This is consistent with the simulation results of the fracture mode for pure Ni with grain size below 15 nm [23]. It has been reported that the fracture

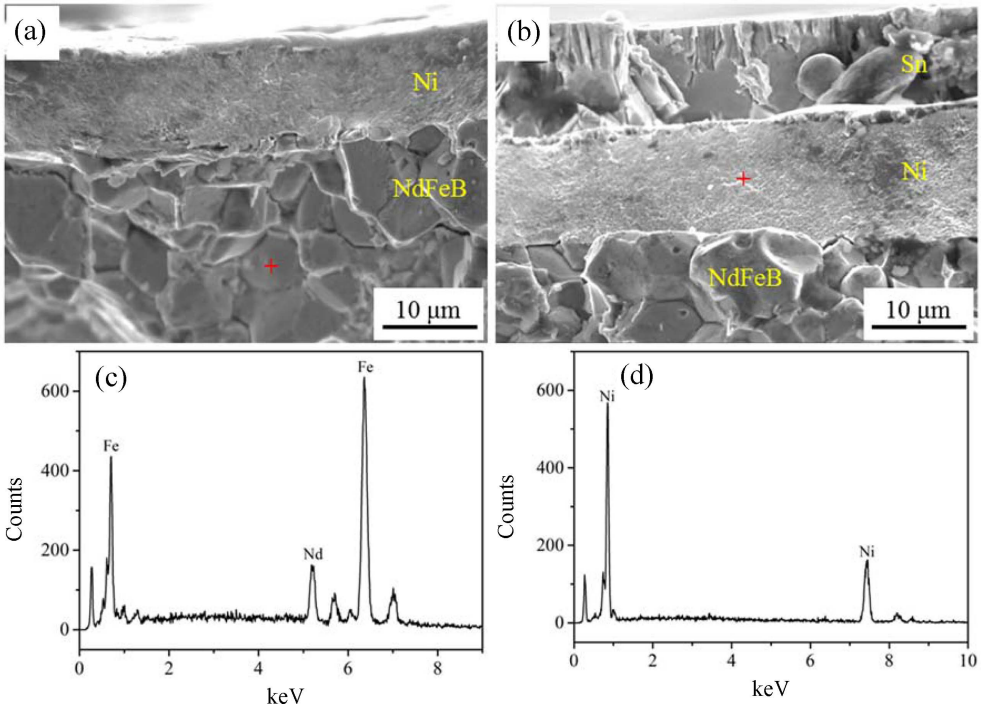

Fig. 6. (Color online) Fractography of (a) Ni and (b) Ni/Sn coated NdFeB magnets and EDS analyses of (c) NdFeB substrate and (d) Ni layer in Ni/Sn bilayer coating.

mode of nanocrystalline FCC metals are grain-size dependent [24, 25]. When the grain size is reduced to a certain extent, the dislocation sources and piles-up are limited and difficult to exist in the grains. As a consequence, the dominant deformation mechanism transforms form the conventional dislocation activity to the grain boundary (GB) sliding (GB-mediated deformation). Likewise, the underlying Ni coating in Fig. 6(b), compositionally analyzed by the EDS method in Fig. 6(d), presents the similar fracture morphology and mode to the Ni coating in Fig. 6(a). This further indicates their same crystal structure and microstructure under the same preparation conditions. However, the top Sn coating in Fig. 6(b) shows the evident difference in the fracture morphology compared to Ni coating. The fracture surface of Sn coating exhibits some cleavage river patterns and no dimple patterns, featuring the typical cleavage fracture. This may be related to the crystallographic and mechanical characteristics of Sn metal with BCT structure. BCT can be considered as a distorted body-centered cubic (BCC) structure, so it may also have the similar intrinsic nature of easy cleavage to BCC structure. Therefore, Ni and Sn coatings exhibit the different fracture mechanisms, which also results in their different contributions to the impact toughness of NdFeB magnet.

For avoiding the effect of coating thickness on the impact toughness, the average thicknesses of various coatings are controlled to be almost same. Both Ni coatings in Figs. 6(a) and (b) are prepared under the same conditions and with the similar average thicknesses of 11 μm and 11.64 μm, respectively, thus they may provide the same contribution to the impact toughness of NdFeB magnet. This suggests that 33.8 % improvement in impact toughness may result from the Ni coating in Ni/Sn bilayer coating. Accordingly, the improvement of impact toughness induced by an additional single Sn coating with the almost same thickness (10.56 μm) as Ni coating can be achieved, and is only about 7.8 %, which is far less than the contribution of Ni coating to impact toughness of NdFeB magnet. Because of the almost same average thickness of Sn and Ni coating, the huge differences between their toughening effects further verify their different fracture mechanisms resulting from their different crystal structures, textures and microstructures as mentioned above.

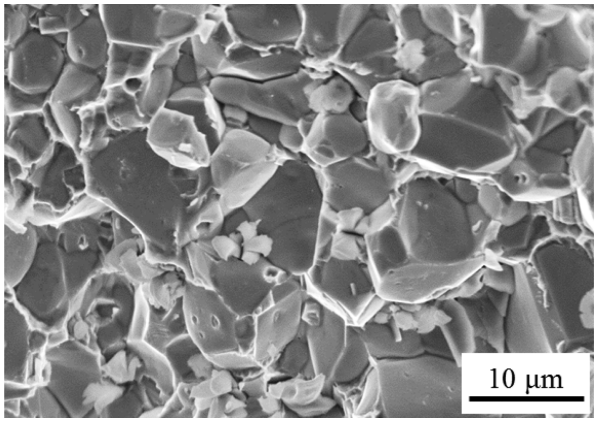

Fig. 7. Fractography of original NdFeB magnet.

3.3. Enhanced mechanism of impact toughness

A comparison of the impact toughness and fracture modes of original and coated magnets clearly reveals that the impact toughness is closely related to the surface coating and its fracture behavior. The impact toughness can be effectively enhanced through the metallic coating probably due to the additional energy absorption generated by its collaborative fracture with the magnet.

The fracture surface of coated NdFeB magnet has presented the better interface combination between either the coatings or the coating and NdFeB magnet. This

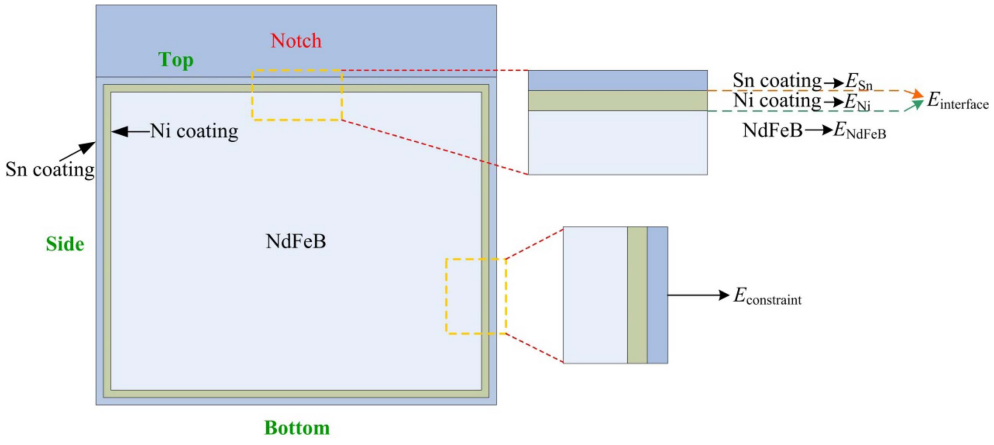

Fig. 8. (Color online) Schematic illustration of the enhanced mechanism for Ni/Sn coated NdFeB magnet.

indicates that the coating has deformed and fractured with the magnet under the impact loading. So the failure of coated magnet includes the fractures of both coating and magnet. Herein, take Ni/Sn coated NdFeB magnet as an example, the schematic illustration of enhance mechanism is shown in Fig. 8. It can be found that the whole fracture surface is composed of three different fracture zones of the Ni, Sn coatings and NdFeB magnet. The formation of each fracture zone all needs to absorb corresponding energy for fulfilling the crack initiation and propagation. The absorbed energy by Ni and Sn coatings on the top and bottom surface of the magnet can be marked as E_{Ni} and E_{Sn}, and E_{Ni} should be greater than E_{Sn}. Similarly, the absorbed energy by NdFeB magnet fracture is labeled as E_{NdFeB}. Moreover, when the crack propagates through the interfaces between Sn and Ni or Ni and NdFeB, it will experience a change in crystallographic structure, microstructure and mechanical properties. As a result, the crack tip will be blunted by plastic deformation, and the crack path will be deflected near the interfaces [26-29]. In this case of Ni/Sn coated NdFeB magnet, the blunting of crack tip can be induced by the plastic deformation of Ni coating when the crack goes through Sn to Ni or NdFeB to Ni. Also, the crack path may be deflected at the interfaces between Sn and Ni or Ni and NdFeB due to their different elasticities and microstructures. Consequently, the crack propagation can be inhibited by the interface and the additional energy needs to be absorbed and consumed for making the crack spread from one material to the adjacent one. In addition, as the crack propagates in NdFeB magnet, it is also constrained by the Ni and Sn coatings on the side of magnet, thereby increasing the energy dissipation for the crack propagation. Therefore, the crack propagation also needs to overcome the interface inhibition and lateral constraints. The absorbed energies correspond to $E_{interface}$ and $E_{constraint}$, respectively. In sum, the total energy absorption E_{tot}(Ni/Sn) of the Ni/Sn coated magnet during fracture can be expressed as follows:

$$E_{tot}(\text{Ni/Sn}) = E_{Sn} + E_{Ni} + E_{NdFeB} + E_{interface} + E_{constraint} \quad (2)$$

where E_{Sn}, E_{Ni} and E_{NdFeB} are the absorbed energy for fracture of Sn, Ni coatings and NdFeB magnet, $E_{interface}$ and $E_{constraint}$ are the absorbed energy for overcoming the interface barrier and lateral constraints. According to Eq. (2), E_{tot}(Ni) and E_{tot}(NdFeB) for Ni coated and original NdFeB magnets can also be deduced, respectively. Considering that both Ni coatings with similar thickness in Ni/Sn and Ni coated NdFeB magnets are prepared under the same conditions, it can be concluded by comparison that E_{tot}(Ni/Sn) > E_{tot}(Ni) > E_{tot}(NdFeB). This sequence relationship is well consistent with the measured results of impact toughness. Besides, the residual compressive stress can be formed during electrodeposition process [30], which is also beneficial to the impact toughness. The available experimental and theoretical analyses illustrate that the toughness of brittle NdFeB magnet can be further improved through extrinsic toughening of the metallic coating.

4. Conclusions

(1) The Ni and Sn coatings exhibit different surface morphologies, which have FCC and BCT crystal structure, respectively. The largest *TC*(hkl) of Ni and Sn coating are obtained at (111) and (112) peaks, indicating their preferred crystal orientation along [111] and [112] directions. Moreover, the average grain size of Ni coating is much smaller than that of Sn coating.

(2) The impact toughness of NdFeB magnet is effectively improved by Ni and Ni/Sn bilayer coatings. The improvement induced by Ni/Sn bilayer coating attains 41.6 %, slightly greater than 33.8 % induced by Ni coating, suggesting the different contribution to the impact toughness of Ni and Sn coatings with different crystallographic structures and microstructures.

(3) The fracture morphologies and modes of the Ni, Sn coatings and NdFeB substrate are distinct. NdFeB substrate and Ni coating both appear intergranular fracture, but their fracture mechanisms are different. The former is mainly due to its weak Nd-rich phase along the grain boundaries, whereas the latter primarily results from the limitation of dislocation activity in the smaller nanosized grains. However, Sn coating exhibits the cleavage fracture owing to its BCT structure.

(4) The enhanced mechanism of impact toughness is analyzed from the point view of the energy absorption during fracture. The expression of total energy absorption for the fracture of the coated NdFeB magnet is tentatively proposed. This deduces the relationship of E_{tot}(Ni/Sn) > E_{tot}(Ni) > E_{tot}(NdFeB), and well explains the experimental results of impact toughness.

Acknowledgments

This work was supported by National Natural Science Foundation of China (Nos. 51401087, 51505198 and 51622104), China Postdoctoral Science Special Foundation (No. 201104511), Jiangsu Government Scholarship for Overseas Study, Natural Science Foundation of Fujian Province of China (No. 2017J01477), the project from the Research Starting-Foundation of Jiangsu University (No.

10JDG030), and Open Fund of Jiangsu Province Key Laboratory of Tribology (No. Kjsmcx2012002).

References

[1] M. Sagawa, S. Fujimura, N. Togawa, H. Yamamoto, and Y. Matsuura, J. Appl. Phys. **55**, 2083 (1984).
[2] T. T. Sasaki, T. Ohkubo, Y. Une, H. Kubo, M. Sagawa, and K. Hono, Acta Mater. **84**, 506 (2015).
[3] T. Ma, B. Wu, Y. Zhang, J. Jin, K. Wu, S. Tao, W. Xia, and M. Yan, J. Alloys Compd. **721**, 1 (2017).
[4] X. G. Cui, C. Y. Cui, X. N. Cheng, X. J. Xu, T. Y. Ma, M. Yan, and C. Wang, J. Alloys Compd. **563**, 161 (2013).
[5] J. W. Kim, S. H. Kim, and Y. D. Kim, Mater. Sci. Eng. A **535**, 325 (2012).
[6] W. Li, A. Li, H. Wang, W. Pan, and H. Chang, J. Appl. Phys. **105**, 07A703-1 (2009).
[7] M. Yan, L. Q. Yu, J. M. Wu, and X. G. Cui, J. Magn. Magn. Mater. **306**, 176 (2006).
[8] S. Liu, D. Cao, R. Leese, S. Bauser, G. Kuhl, J. Liu, M. Walmer, and E. Kottcamp, Proc. 17th Int. Workshop Rare-Earth Magnets and Their Application, 360 (2002).
[9] H. J. Wang, A. H. Li, Y. Q. Guo, M. G. Zhu, and W. Li, J. Appl. Phys. **103**, 07E119-1 (2008).
[10] H. J. Wang, A. H. Li, M. G. Zhu, and W. Li, J. Magn. Magn. Mater. **307**, 268 (2006).
[11] Z. H. Hu, M. G. Zhu, W. Li, and F. Z. Lian, J. Magn. Magn. Mater. **320**, 96 (2008).
[12] J. Liu, P. Vora, M. Walmer, E. Kottcamp, S. Bauser, A. Higgins, and S. Liu, J. Appl. Phys. **97**, 10H101-1 (2005).
[13] M. Yue, A. L. Cao, G. P. Wang, W. Q. Liu, and J. X. Zhang, Phys. Status Solidi A **204**, 4149 (2007).
[14] P. Zhang, G. Xu, J. Liu, X. Yi, Y. Wu, and J. Chen, Appl. Surf. Sci. **363**, 499 (2016).
[15] J. Ding, B. Xu, and G. Ling, Appl. Surf. Sci. **305**, 309 (2014).
[16] E. Isotahdon, E. Huttunen-Saarivirta, V. T. Kuokkala, M. Paju, and L. Frisk, J. Alloys Compd. **585**, 203 (2014).
[17] W. J. Chou, G. P. Yu, and J. H. Huang, Surf. Coat. Technol. **149**, 7 (2002).
[18] X. Ren, W. Dang, Q. Ma, X. Zhu, W. Zi, L. Jia, B. Liu, X. Zhang, F. Xiao, and H. Yang, Sol. Energy **125**, 192 (2016).
[19] M. R. Vaezi, S. K. Sadrnezhaad, and L. Nikzad, Colloids Surf. A **315**, 176 (2008).
[20] Y. Wang, C. Yang, J. He, W. Wang, N. Mitsuzak, and Z. Chen, Appl. Surf. Sci. **372**, 1 (2016).
[21] Y. D. Wang, Thesis, University of California, Los Angeles, 2016.
[22] J. D. Giallonardo, U. Erb, K. T. Aust, and G. Palumbo, Philos. Mag. **91**, 4594 (2011).
[23] D. Farkas, H. V. Swygenhoven, and P. M. Derlet, Phys. Rev. B **66**, 340 (2002).
[24] S. Yip, Nat. **391**, 532 (1998).
[25] Z. Shan, E. A. Stach, J. M. Wiezorek, J. A. Knapp, D. M. Follstaedt, and S. X. Mao, Sci. **305**, 654 (2004).
[26] Y. Huang and H. W. Zhang, Acta Metall. Mater. **43**, 1523 (1995).
[27] Y. Sugimura, P. G. Lim, C. F. Shih, and S. Suresh, Acta Metall. Mater. **43**, 1157 (1995).
[28] K. S. Chan, M. Y. He, and J. W. Hutchinsson, Mater. Sci. Eng. A **167**, 57 (1993).
[29] M. Y. He, F. E. Heridia, D. J. Wissuchek, M. C. Shaw, and A. G. Evans, Acta Metall. Mater. **43**, 1223 (1992).
[30] S. J. Hearne and J. A. Floro, J. Appl. Phys. **97**, 014901-1 (2005).